

# The impact of SCIAMACHY near-infrared instrument calibration on CH<sub>4</sub> and CO total columns

A. M. S. Gloudemans<sup>1</sup>, H. Schrijver<sup>1</sup>, Q. Kleipool<sup>1,\*</sup>, M. M. P. van den Broek<sup>1</sup>, A. G. Straume<sup>1,\*\*</sup>, G. Lichtenberg<sup>1</sup>, R. M. van Hees<sup>1</sup>, I. Aben<sup>1</sup>, and J. F. Meirink<sup>2</sup>

<sup>1</sup>SRON National Institute for Space Research, Utrecht, The Netherlands

<sup>2</sup>Royal Netherlands Meteorological Institute (KNMI), De Bilt, The Netherlands

\* now at: Royal Netherlands Meteorological Institute (KNMI), De Bilt, The Netherlands

\*\* now at: the European Space Agency, European Space Research & Technology Centre (ESA-ESTEC), Noordwijk, The Netherlands

Received: 9 February 2005 – Published in Atmos. Chem. Phys. Discuss.: 18 March 2005

Revised: 26 July 2005 – Accepted: 25 August 2005 – Published: 14 September 2005

**Abstract.** The near-infrared spectra measured with the SCIAMACHY instrument on board the ENVISAT satellite suffer from several instrument calibration problems. The effects of three important instrument calibration issues on the retrieved methane (CH<sub>4</sub>) and carbon monoxide (CO) total columns have been investigated: the effects of the growing ice layer on the near-infrared detectors, the effects of the orbital variation of the instrument dark signal, and the effects of the dead/bad detector pixels. Corrections for each of these instrument calibration issues have been defined. The retrieved CH<sub>4</sub> and CO total columns including these corrections show good agreement with CO measurements from the MOPITT satellite instrument and with CH<sub>4</sub> model calculations by the chemistry transport model TM3. Using a systematic approach, it is shown that all three instrument calibration issues have a significant effect on the retrieved CH<sub>4</sub> and CO total columns. However, the impact on the CH<sub>4</sub> total columns is more pronounced than for CO, because of its smaller variability. Results for three different wavelength ranges are compared and show good agreement. The growing ice layer and the orbital variation of the dark signal show a systematic, but time-dependent effect on the retrieved CH<sub>4</sub> and CO total columns, whereas the effect of the dead/bad pixels is rather unpredictable: some dead pixels show a random effect, some more systematic, and others no effect at all. The importance of accurate corrections for each of these instrument calibration issues is illustrated using examples where inaccurate corrections lead to a wrong interpretation of the results.

## 1 Introduction

The SCanning Imaging Absorption spectroMeter for Atmospheric CHartographY (SCIAMACHY)<sup>1</sup> which was launched on board the ENVISAT satellite on 1 March 2002, has allowed the measurement of global distributions of methane (CH<sub>4</sub>) and carbon monoxide (CO) down to the Earth's surface. These gases play an important role in tropospheric chemistry and possible climate change. Therefore, a good knowledge of the global distributions of these gases is a prerequisite to fully understand their role in atmospheric chemistry.

Global measurements of CH<sub>4</sub> and CO have also been performed by the MOPITT instrument on board the EOS-TERRA satellite in the near- and thermal infrared (e.g. Drummond and Mand, 1996; Deeter et al., 2003). Up till now, MOPITT has been unsuccessful in retrieving accurate CH<sub>4</sub> total columns from their data. Methane and carbon monoxide have been measured earlier by the Interferometric Monitoring of Greenhouse Gases (IMG) instrument on board the ADEOS satellite (Clerbaux et al., 2003; Barret et al., 2005). Recently, the EOS-AURA satellite was launched, carrying the Tropospheric Emission Spectrometer (TES) instrument, which is currently measuring CH<sub>4</sub> and CO (e.g. Beer et al., 2001). However, retrieved total column products from this instrument are not yet available. Ground-based measurements of CO and CH<sub>4</sub> total columns are available from a number of ground stations, but they do not provide global coverage and a significant fraction of these are at elevated locations. Thus, these stations only measure the total column directly above the station, whereas the larger spatial coverage of a SCIAMACHY ground pixel will mostly also include

Correspondence to: A. M. S. Gloudemans  
(a.gloudemans@srn.nl)

<sup>1</sup><http://envisat.esa.int/instruments/sciamachy/>

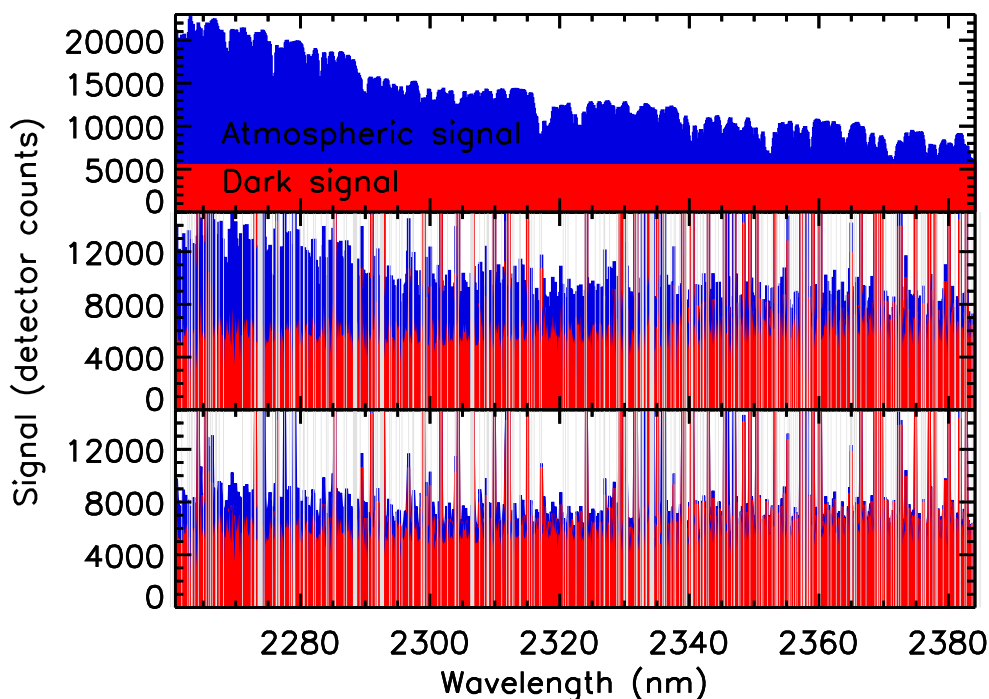


**Fig. 1.** The total signal, i.e. dark signal+atmospheric signal, as measured by SCIAMACHY's channel 8 detector. The total dark signal is shown in red, the atmospheric signal in blue. The white vertical lines denote the positions of the dead detector pixels at the end of February 2004. Top: Simulated SCIAMACHY measurement in the case of a strong atmospheric signal, assuming a noise-free dark signal. Middle: SCIAMACHY measurement over the Sahara with a high surface albedo of 0.55. The relative contribution of the dark signal of the SCIAMACHY instrument to the total measured signal varies from  $\sim 45\%$  at 2260 nm to  $\sim 75\%$  at 2380 nm. Bottom: SCIAMACHY measurement over Central Africa with a lower surface albedo of 0.11. The relative contribution of the dark signal of the SCIAMACHY instrument to the total measured signal varies from  $\sim 63\%$  at 2260 nm to  $\sim 97\%$  at 2380 nm.

contributions from lower (polluted) altitudes, where most of the CO and CH<sub>4</sub> resides (de Mazière et al., 2004; Dils et al., 2005).

The retrievals of CO and CH<sub>4</sub> from SCIAMACHY's near-infrared channel 8 have proven more complex than anticipated, due to the presence of an unexpected ice layer on the detectors, which varies in time. Its effects have been reduced by applying dedicated in-flight decontamination procedures and additional in-flight calibration measurements, as well as improvements to the calibration. However, the quantitative effects of these problems on the retrieved CH<sub>4</sub> and CO total columns have only been investigated for very few cases.

This paper focuses on a more systematic investigation of some of the major calibration problems concerning SCIAMACHY's near-infrared channel 8 and the effects of these problems on the retrieved CH<sub>4</sub> and CO total columns from this channel. The problems addressed in this paper are at present not or insufficiently corrected for in the operational SCIAMACHY data provided by ESA/DLR.

Different corrections for these issues have been developed independently by a number of research groups (e.g. Buchwitz et al., 2004b; Frankenberg et al., 2005b; Gloudemans et al., 2004), but the detailed information describing the applied corrections and their impact is often lacking.

Model calculations show that in order to determine e.g. CH<sub>4</sub> sources and sinks, and estimate CO emissions from SCIAMACHY measurements, a precision of  $\sim 1\text{--}2\%$  for CH<sub>4</sub> and  $\sim 10\text{--}20\%$  for CO is required (e.g. Ehret and Kiemle, 2005, S. Houweling and M. Krol, SRON/IMAU, private communication). This paper shows that in order to retrieve total columns with those precisions from channel 8, detailed corrections for all known instrument calibration problems are required. Section 2 discusses the major instrument calibration problems, Sect. 3 describes the retrieval algorithm used, and Sect. 4 shows the retrieval results using SCIAMACHY measurements. The effects of the instrument calibration improvements on the retrieved CH<sub>4</sub> and CO total columns are presented in Sect. 5 as well as comparisons of retrievals in different spectral windows of SCIAMACHY's channel 8. Finally, Sect. 6 discusses all results and the conclusions are summarized in Sect. 7.

## 2 Instrument calibration

The near-infrared nadir spectra measured by SCIAMACHY's channel 8 (2265 to 2380 nm) contain absorption lines of CH<sub>4</sub>, CO, H<sub>2</sub>O, and N<sub>2</sub>O. However, the retrieval of

these species in this wavelength range is complicated due to the low atmospheric signal compared to the instrument dark signal itself (Fig. 1). This dark signal is the sum of the detector dark signal and the thermal background of the instrument and represents the total measured signal when no light is falling onto the instrument itself. SCIAMACHY measurements show that in case of a strong atmospheric signal, corresponding to a surface albedo of 0.55, the dark signal contribution varies from  $\sim 45\%$  at the short wavelength end of channel 8 to  $\sim 75\%$  at the long wavelength end. In the case of a lower surface albedo, the corresponding lower atmospheric signal results in an even higher contribution of the dark signal as is shown in Fig. 1. Thus, an accurate instrument calibration (dark signal etc.) is required in order to retrieve meaningful total columns from SCIAMACHY's channel 8.

Unfortunately, the retrieval within this wavelength range is hampered by a number of instrument-calibration problems. The most important complication in channel 8 is the growth of an ice layer on the detector. This ice layer is due to spurious water absorbed in the ENVISAT satellite frame. Over time, this water evaporates and most of it escapes to space. However, a small portion is trapped by the SCIAMACHY instrument isolation blankets and freezes out onto the near-infrared detectors. The ice layer increases slowly in time up to a thickness of  $\sim 400\ \mu\text{m}$  and leads to losses in the total measured signal of up to  $\sim 50\%$  (Lichtenberg et al., 2005). This loss in signal is partially alleviated by heating the detector every 3–6 months, hereby evaporating the ice layer. However, the decrease of the signal behaves differently after each of these decontamination periods (see Fig. 2 and <http://atmos.af.op.dlr.de/projects/scops/> or <http://www.sron.nl/www/code/eos/sciamachy/calibration/SCIACALtransmission.php>). The consequences of the growing ice layer are threefold:

- The signal-to-noise ratio of the spectra is reduced.
- The instrument thermal background contribution to the total dark signal decreases, as the ice layer also absorbs these photons. In order to deal with this, the total dark signal has been measured every orbit, since October 2002 (Kleipool, 2003a).
- Scattering of light in the ice layer gives rise to extended wings in the slit function.

The latter has a significant effect on the retrieved columns and is the most difficult to correct for, since it varies in time and cannot be determined independently. One possibility to determine a correction for this broadening of the slit function is by using the in-flight measurements from SCIAMACHY's Spectral Light Source (SLS), which clearly show the presence of broadened wings over time. However, this spectral lamp does not illuminate the whole slit and the overlapping line wings in the SLS spectra complicate the use of these measurements to correct for the broadening of the slit function. In addition, the ice layer is not uniform over the whole

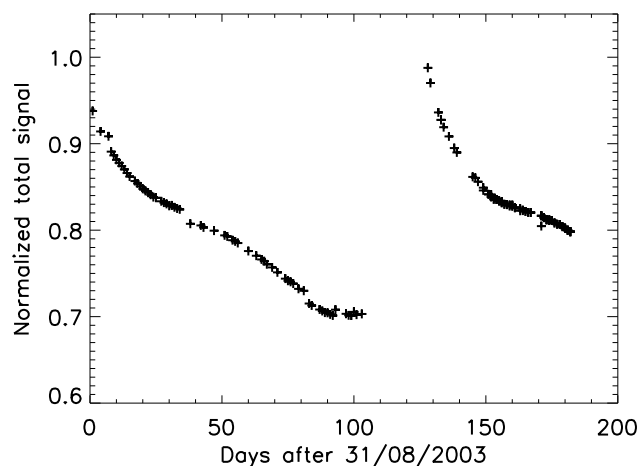


**Fig. 2.** The measured total signal averaged over channel 8 and normalised to an (almost) ice-free measurement in August 2002. Only data right after the August 2003 decontamination (duration: 375 h) till the end of February 2004 are shown and include the decontamination period in December 2003/January 2004 (duration: 338 h). The loss in the total signal due to the growing ice layer in SCIAMACHY's channel 8 can be clearly seen.

channel, so that defining a correction method which is applicable at all wavelengths within channel 8 is complicated. Therefore, a different approach has been adopted in the retrievals presented here, which is described in Sect. 3.

Furthermore, the instrument thermal background and thus the total dark signal also varies within an orbit. This is due to the optical bench heating up on the day side of the orbit. The dark signal is measured upon entering the eclipse near the South Pole, where the contribution of the thermal background signal is largest. This ultimately leads to CH<sub>4</sub> total columns that are too high, especially at high Northern latitudes where the actual dark signal deviates most from the measured dark signal (Kleipool, 2004a). The deviation from the measured dark signal varies over the months, since the dark signal is influenced by the thickness of the ice layer.

Lastly, the near-infrared wavelength range in channel 8 is sampled by 1024 detector pixels, a significant fraction of which have turned “dead” or “bad” during the life time of SCIAMACHY (Kleipool, 2004b). A pixel is labelled “dead” when there is no spectral response and “bad” when the spectral response is too noisy or unpredictable. Since neither “dead” nor “bad” detector pixels should be used in the retrievals, both will be referred to as “dead” pixels throughout this paper for simplicity. The most likely causes for this failure of detector pixels are the manufacturing process itself and in-flight radiation damage (Kleipool et al., 2005<sup>2</sup>). The most worrying consequence of this is that the number of dead

<sup>2</sup>Kleipool, Q., Jongma, R., Gloudemans, A. M. S., et al.: In-flight radiation induced degradation of the SCIAMACHY extended wavelength InGaAs near-infrared detectors, in preparation, 2005.

pixels appears to be increasing steadily in time, at a rate of ~60 pixels per year. This calls for a time-dependent dead pixel mask to be used in the retrieval codes when retrieving total columns from channel 8. In Sect. 5.3 it will be shown that using one dead pixel in the retrieval code, can lead to erroneous results (see also Kleipool, 2004b).

### 3 Retrieval algorithm

The retrieval method used here is based on an Iterative Maximum Likelihood Method (IMLM) and has been developed at SRON. The retrieval uses a fixed set of climatological atmospheric profiles based on the US standard atmosphere (1976) to compute a model spectrum in terms of optical depths. For each SCIAMACHY ground pixel these profiles are truncated at the mean surface elevation of the pixel.

Once the optical depths are calculated, the earth radiance can be computed in a forward model (Schrijver, 1999, Gloudemans et al., 2005<sup>3</sup>), which is then transformed by an instrument model to represent the radiation detected by the instrument detectors. This modelled spectrum is then fitted – by adjusting the total columns of the different species – to the measured (detector) spectrum in an iterative way. The instrument model also provides an estimate of the instrument noise, from which, by standard statistical methods, an estimate is computed of the instrument-noise related errors in the total columns. A more detailed description of the retrieval algorithm can be found in Schrijver (1999) and Gloudemans et al. (2005<sup>3</sup>).

The instrument model used in the current retrievals includes a dedicated time-dependent dead pixel mask, as well as dark signals for every orbit, both of which are taken from the SRON database set up by Kleipool (2003a, 2004b). A correction for the variation of the dark signal within an orbit is also included (Kleipool, 2004a), as well as a first approximate correction for the broadening of the slit function due to the growing ice layer. Comparing SLS spectra for different thicknesses of the ice layer shows that the effect of the slit function's extended wings on the spectrum resembles an additional background signal. Therefore, this latter correction involves adding a constant baseline per orbit (i.e. independent of wavelength) to the modelled detector spectrum, which has been calculated from a slit function measured under (almost) ice-free conditions. Since only a small spectral window of channel 8 is used in the retrievals presented here, this appears to be an acceptable approximation, as can also be shown by computing synthetic spectra. The size of the additional background signal relative to the total measured signal has been determined by fixing the SCIAMACHY CH<sub>4</sub> values on a daily basis to the CH<sub>4</sub> total columns over the central part

of the Sahara between 20° W and 20° E, as calculated by atmospheric chemistry models. These models show little variation in the CH<sub>4</sub> total columns in space and time over this part of the Sahara and are in good agreement with in situ measurements at the Assekrem station in Algeria (S. Houweling 2005, private communication). Therefore it appears a good region for calibrating the SCIAMACHY data. Despite the generally good agreement with in situ and flask measurements on a global scale (e.g. Houweling et al., 1999, 2000), these models may deviate from reality. Since averages over a relatively large geographical area are taken, the resulting bias in the retrieved CH<sub>4</sub> total columns is estimated to be not more than 1–2%.

All above correction methods, except for the correction for the broadening of the slit function's wings, are the same as those included in the SCIAMACHY level 1b products patched by SRON<sup>4</sup>. It is still under investigation how these correction methods can be refined, but further improvements are expected to be small compared to the effects shown in Sect. 5. In addition, a number of improvements to the retrieval approach are foreseen. For example, only a fixed atmospheric temperature profile, the US standard temperature profile, has been used at present, but at the time of writing the inclusion of an ECMWF temperature profile in the IMLM retrieval algorithm is being implemented. The lack of a correct temperature profile can lead to errors in the retrieved CO total column of  $<0.35 \times 10^{18}$  molec/cm<sup>2</sup> for most ground pixels, smaller than the current instrument-noise related precision of the retrievals. The CH<sub>4</sub> total columns are mostly off by <5% with a maximum error of ~10% for some isolated cases (Gloudemans et al., 2005<sup>3</sup>). However, this does not affect the effect of the instrument calibration problems presented here, since these are shown as the difference between retrievals with and without correction, both of which use the same temperature profile. Recently, retrievals using ECMWF temperature profiles have been performed for part of the data set presented here. These show indeed that the effects shown in Sect. 5 are not affected by using the fixed US standard temperature profile. Scattering in the atmosphere is not included in the forward model, but is expected to introduce only small corrections of <1% for CH<sub>4</sub> and <2% for CO (Buchwitz and Burrows, 2004). The retrieved CH<sub>4</sub> and CO total column data presented in this paper have been cloud masked and thus contain only cloud-free measurements. For this, a cloud mask based on the SCIAMACHY Polarisation Measurement Devices (PMDs) 2, 3, and 4 has been included in the IMLM algorithm. This cloud algorithm is similar to that described by Krijger et al. (2005), except that the distinction between ice/snow covered surfaces is not included. The cloud mask by Krijger et al. (2005) is being implemented at the time of writing.

<sup>3</sup>Gloudemans, A. M. S., Schrijver, H., and Jongma, R.: The Iterative Maximum Likelihood Method (IMLM) for near-infrared trace gas retrieval from SCIAMACHY, in preparation, 2005.

<sup>4</sup>[http://www.sron.nl/~richardh/SciaDC/scia\\_patch\\_1b/index.html](http://www.sron.nl/~richardh/SciaDC/scia_patch_1b/index.html)

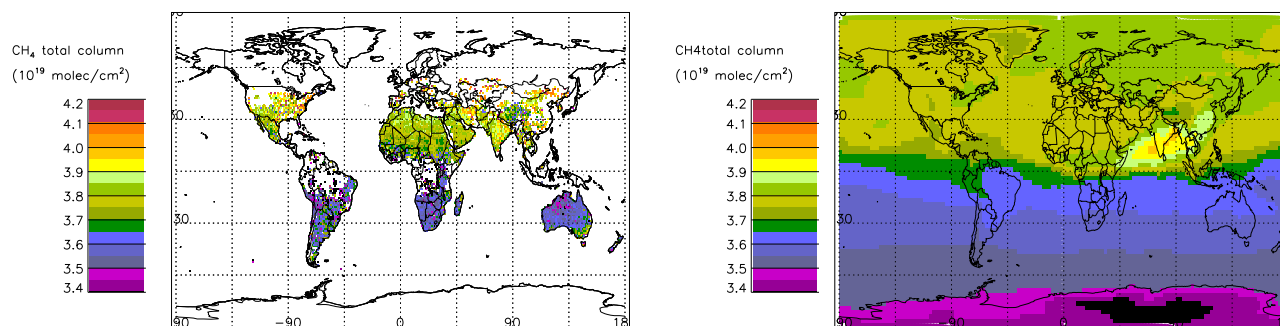


**Fig. 3.** Monthly averaged CH<sub>4</sub> total columns for November 2003. Left panel: Retrieval results from the IMLM algorithm. Only cloud-free individual SCIAMACHY ground pixels, with instrument-noise related errors  $<0.2 \times 10^{19} \text{ cm}^{-2}$  have been averaged and re-gridded on a  $1^\circ \times 1^\circ$  grid. The CH<sub>4</sub> total columns have been normalized to surface elevation prior to averaging. Right panel: Total columns calculated from the chemistry transport model TM3 on a  $2.5^\circ$  by  $2.5^\circ$  horizontal grid. The total columns have been normalized to surface pressure.

#### 4 Retrieval results

Near-infrared CH<sub>4</sub> and CO total columns from SCIAMACHY have also been reported by others (e.g. Buchwitz et al., 2004a,b, 2005; Frankenberg et al., 2005a,c). Qualitative comparisons have shown that the IMLM results agree well with these other data products (e.g. Gloudemans et al., 2004), even though there are significant differences between the algorithms used and the applied instrument calibration.

In order to investigate the effects of the different instrument calibration problems mentioned in Sect. 2 on the retrieved CH<sub>4</sub> and CO total columns, six months of SCIAMACHY channel 8 data have been analysed. The period September 2003 – February 2004 has been chosen, because the available data result in a good global coverage. The start of this period is right after the August 2003 decontamination (duration: 375 h) and also includes the decontamination period in December 2003/January 2004 (duration 338 h), allowing the investigation of instrument-calibration effects after two different decontamination procedures. Results are shown for retrievals in the channel 8 spectral window between 2321–2334 nm. This window is similar to that used by Frankenberg et al. (2005a). Results for two other spectral windows of channel 8 are discussed in Sect. 5.4. The data presented in this section include corrections for all instrument-calibration problems mentioned in Sect. 2. Section 5 illustrates in more detail the effects on the retrieval of not including these corrections.

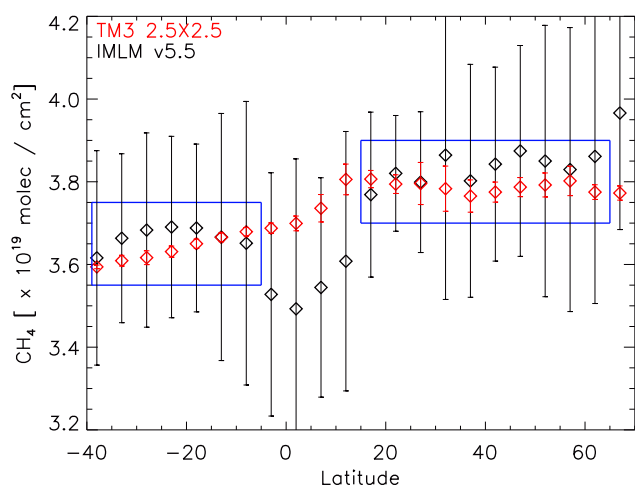
##### 4.1 CH<sub>4</sub>

Figure 3 shows the monthly-averaged CH<sub>4</sub> results for November 2003. Only cloud-free ground pixels with a high enough signal-to-noise ratio have been included in the SCIAMACHY retrievals. The lack of data over the oceans is due to the fact that the surface albedo is too low, resulting in a signal-to-noise ratio which is too small to perform accurate

retrievals. At high latitudes ( $\geq 70^\circ \text{ N}$ ) the signal-to-noise ratio is also too low.

Unfortunately, no independent satellite-based CH<sub>4</sub> total column measurements are available, so that the SCIAMACHY CH<sub>4</sub> total columns can only be compared to total columns from ground-based stations or calculations from atmospheric chemistry transport models. Comparisons of the IMLM total columns with ground-based measurements are presented by Dils et al. (2005), but these do not provide global coverage. Therefore in Fig. 3, the retrieved CH<sub>4</sub> total columns are compared with calculations by the chemistry transport model TM3 from the Royal Netherlands Meteorological Institute (KNMI). A detailed description of the TM3 model used here can be found in Dentener et al. (2003) and references therein. The model includes CH<sub>4</sub> emissions closely following Houweling et al. (1999). These model calculations show a good agreement with in situ measurements (<http://www.cmdl.noaa.gov/ccg/>) and reproduce the background CH<sub>4</sub> levels well. Although most chemistry transport models do not contain up-to-date emissions and the model resolution is mostly coarser than the resolution of the SCIAMACHY ground pixels (e.g.  $2^\circ$  by  $3^\circ$  as opposed to  $120 \times 30 \text{ km}$ , i.e.  $\sim 1.1^\circ$  by  $0.27^\circ$  at the equator) they do provide accurate information on the large scale distribution of CH<sub>4</sub>, such as the North-South gradient and well-known continuous or seasonal sources and sinks.

Figure 3 shows that such a qualitative comparison shows good agreement between the monthly-averaged SCIAMACHY data and the corresponding TM3 calculations. For instance, the North-South gradient is clearly visible in the SCIAMACHY data. In addition, many differences can be identified as well, such as the areas in Eastern USA, and the East coast of Australia, which are hardly visible in the TM3 model. The origin of these differences is still under investigation. In Central Africa between  $\sim 10^\circ \text{ S}$  and  $\sim 5^\circ \text{ N}$  a region with low CH<sub>4</sub> columns is visible which is not in agreement with the TM3 calculations. Since this region is mostly cloudy during this time of the year, this is probably due to



**Fig. 4.** Comparison of the monthly averaged CH<sub>4</sub> total columns for September 2003, where all data within a five-degree latitude bin have been averaged (see text). The black diamonds denote the IMLM CH<sub>4</sub> total columns, the red diamonds the corresponding TM3 data. The blue boxes show the regions where the difference between the IMLM and TM3 CH<sub>4</sub> total columns is  $\lesssim 2\%$ . Only cloud-free ground pixels with instrument-noise related errors  $< 0.2 \times 10^{19}$  molec/cm<sup>2</sup> have been included. The error bars denote the  $1\sigma$  standard deviation of the data points averaged within each 5° latitude bin. Both the SCIAMACHY and the TM3 total columns have been normalized to the surface pressure.

cloudy SCIAMACHY ground pixels that have not been filtered out by the cloud mask included in the IMLM retrieval algorithm. Other persistently cloudy areas such as in the Amazon basin are also clearly identified by the lack of cloud-free SCIAMACHY data. In addition, low CH<sub>4</sub> columns are seen in West Africa between  $\sim 5$ – $15^\circ$  N. This area is known for the presence of forest fires and the corresponding smoke may not be picked up by the cloud mask. Smoke and/or clouds shield the CH<sub>4</sub> in the lower parts of the atmosphere, resulting in too low CH<sub>4</sub> total columns measured by SCIAMACHY. Retrieval of CO<sub>2</sub>, another well-mixed gas, from SCIAMACHY's channel 6, also results in too low total columns of a few percent in the same area, using the same cloud mask (W. Hartmann, SRON, private communication).

Figure 4 shows a more quantitative comparison of the monthly-averaged CH<sub>4</sub> total columns from the IMLM retrieval algorithm with TM3 for September 2003. Here, the globe has been divided in five-degree latitude bins. All SCIAMACHY data within each latitude bin have been averaged over the whole month and compared to the monthly average of the collocated TM3 CH<sub>4</sub> total columns within the same latitude bin. Both data sets have been normalized to surface pressure prior to averaging. The results show a good agreement between latitudes  $40^\circ$  S and  $5^\circ$  S and on the Northern Hemisphere ( $\gtrsim 15^\circ$  N). In both regions the difference between the retrieved CH<sub>4</sub> columns and the TM3 calculations

is less than  $\sim 2\%$ , except for the region North of  $65^\circ$  N, where it is  $\sim 5\%$ . This region may suffer from higher solar zenith angles or cloudy ground pixels, resulting in erroneous CH<sub>4</sub> columns. The area between  $5^\circ$  S and  $15^\circ$  N is mostly cloudy at this time of the year, as is also seen for November 2003 in Fig. 3, and may also be affected by smoke from the forest fires, resulting in lower CH<sub>4</sub> total columns and less collocations with TM3.

Although only comparisons for two months, September and November 2003, are shown here, the other months do give similar results (see also Straume et al., 2005).

#### 4.2 CO

Independent satellite-based CO total column measurements are available, unlike for CH<sub>4</sub>. Especially for CO, which has strong temporal and spatial variations, such satellite inter-comparisons provide a very valuable validation technique. The MOPITT instrument is currently the only other instrument from which CO total column measurements from space are available. MOPITT uses gas-correlation spectroscopy, based on pressurized cells (Drummond and Mand, 1996), whereas SCIAMACHY uses a grating spectrometer. In addition, SCIAMACHY measures CO in the near-infrared, while MOPITT observes CO in the thermal infrared, where the CO lines are much stronger than in the near-infrared. Thus, measurements from these satellites provide two independent sets of CO total column products, making them very suitable for a first qualitative comparison with the retrieved SCIAMACHY CO total columns. In the near-infrared, the surface reflectance over the oceans is very low, complicating the SCIAMACHY retrievals in these areas. Measurements in the thermal infrared however have a lower sensitivity to the boundary layer, due to small temperature contrasts with respect to the surface. In those cases, a priori information is added to the MOPITT CO measurements. Since this is more likely to happen at night, only day-time MOPITT measurements are taken into account.

Monthly-averaged results for CO compared with measurements by the MOPITT instrument are shown in Figs. 5 and 6 for November and September 2003. Only cloud-free ground pixels with a high enough signal-to-noise ratio have been included in the SCIAMACHY retrievals shown here.

The SCIAMACHY CO total columns for November 2003 shown in Fig. 5 are in reasonably good agreement with the MOPITT measurements of that month. The data sets show a reasonable agreement on both the Northern and Southern Hemisphere, and enhanced CO columns in West and Central Africa and Brazil due to bio-mass burning are seen in both data sets. Similar enhanced CO columns are reported by Frankenberg et al. (2005a), using the same SCIAMACHY data, but using a different retrieval algorithm (Frankenberg et al., 2005b). This is the same region where the low CH<sub>4</sub> columns are seen in Fig. 3, providing further evidence for

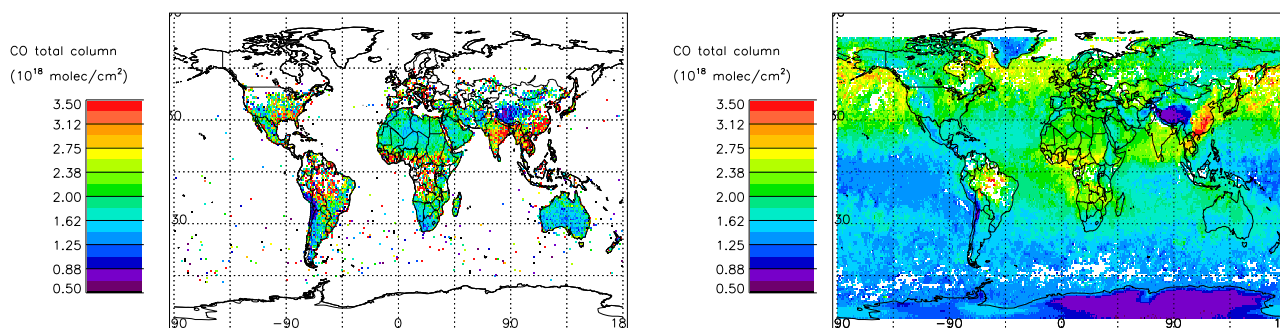


**Fig. 5.** Monthly averaged CO total columns for November 2003. Left panel: Retrieval results from the IMLM algorithm. Only cloud-free individual SCIAMACHY pixels, with instrument-noise related errors  $<1.5 \times 10^{18} \text{ cm}^{-2}$  have been averaged and re-gridded on a  $1^\circ \times 1^\circ$  grid. Right panel: Total columns as measured by the MOPITT instrument (from: NASA Langley Research Center Atmospheric Sciences Data Center). Only daytime measurements have been averaged.

the low CH<sub>4</sub> columns being due to smoke from forest fires (see Sect. 4.1).

Well-known polluted areas, such as in Asia, are also clearly visible in Fig. 5 as regions with enhanced CO total columns. Mountainous areas, such as the Himalayas and the Andes, show up in both the SCIAMACHY and MOPITT measurements as regions with low CO total columns. Large differences are also observed: the forest fires are more pronounced in the SCIAMACHY data than in the MOPITT measurements, and the retrieved SCIAMACHY total columns also show higher CO values over India and Eastern USA. Part of this difference may come from the fact that the MOPITT measurements are less sensitive to the boundary layer resulting in lower CO total columns (Deeter et al., 2003). In this comparison, the difference in the averaging kernels for the MOPITT and SCIAMACHY instrument has not been taken into account. A more detailed comparison of these two sets of satellite measurements is currently planned in close collaboration with the National Center for Atmospheric Research (NCAR).

A somewhat more quantitative comparison of the IMLM CO total columns with MOPITT is shown in Fig. 6. This figure is constructed in a similar way as Fig. 4 for CH<sub>4</sub>. It can be seen that there is a good agreement between the two data sets for September 2003. Differences are generally within 10%, except for the region between  $\sim 0^\circ$  and  $\sim 15^\circ \text{ N}$  where the differences are up to  $\sim 20\%$ . This may be due to the relatively few data points in this area, due to clouds. The standard deviation of the SCIAMACHY measurements is however systematically larger than for the MOPITT data. Part of this may be due to retrieval errors and the rather loose constraints on the signal-to-noise ratio, and part of this may be real: because of the larger sensitivity of SCIAMACHY to the boundary layer, a larger variability in the retrieved CO total columns from individual measurements is expected. A more detailed analysis will help to distinguish between these two.

As is the case for CH<sub>4</sub>, the other months in the period September 2003–February 2004 show similar CO

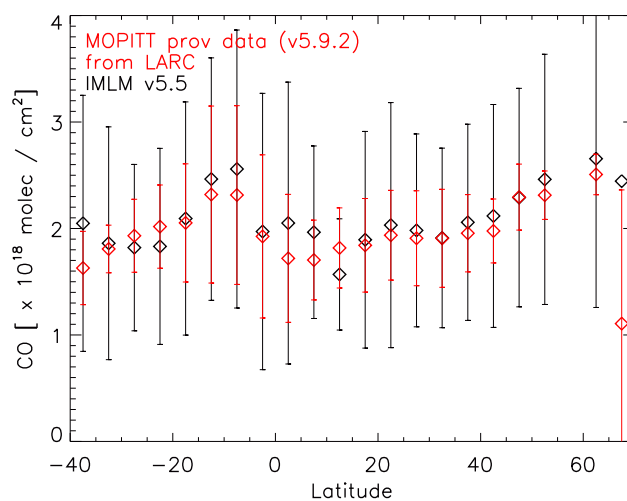


**Fig. 6.** Comparison of the monthly averaged CO total columns for September 2003, where all data within a five-degree latitude bin have been averaged. The black diamonds denote the IMLM CO total columns, the red diamonds the corresponding MOPITT data. Only pixels with a cloud-fraction  $<20\%$  and instrument-noise related errors  $<1.5 \times 10^{18} \text{ molec/cm}^2$  have been included. The error bars denote the  $1\sigma$  standard deviation of the data points averaged within each  $5^\circ$  latitude bin. The MOPITT data are taken from the NASA Langley Research Center Atmospheric Sciences Data Center.

SCIAMACHY–MOPITT comparisons (see also Straume et al., 2005). For January 2004, the quality of the retrieved CO columns cannot be derived from comparisons with MOPITT data, since only a few days of MOPITT data are available for this month.

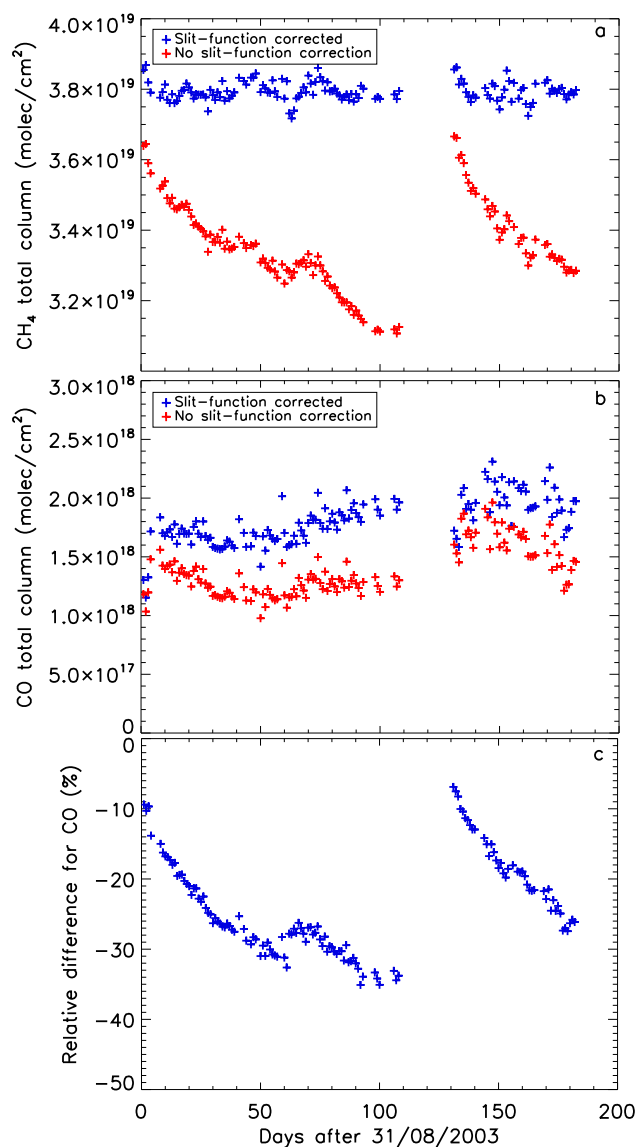


**Fig. 7.** Total columns averaged over the Sahara for each day in the period September 2003–February 2004, with and without applying a correction for the broadening of the slit function due to ice growth on SCIAMACHY's channel 8 detector (see Sect. 3). The gap between day 108 and 131 corresponds to the December 2003 decontamination period. Note that here the whole Sahara is used, whereas the correction for the broadening of the slit function is based only on the central part of the Sahara between 20° W and 20° E. (a) The CH<sub>4</sub> total columns, normalized to the mean surface elevation of the corresponding SCIAMACHY pixel and then averaged over the Sahara region. The trend seen in the CH<sub>4</sub> total columns without the slit-function correction resembles the loss in the total signal due to the ice growth in this period (Fig. 2). (b) The CO total columns. The columns without slit-function correction do not show a clear correlation with the decrease in the total signal for this period, but are nevertheless clearly affected by the broadening of the slit function. (c) Relative difference of the CO total columns without and with applying a slit-function correction respectively, as shown in panel b. The difference in the CO total columns clearly increases as the ice layer becomes thicker.

## 5 Effects of instrument calibration on the retrieved total columns

### 5.1 Effects of the growing ice layer

The effect of the broadening of the slit function due to ice growth on SCIAMACHY's channel 8 detector has been investigated by performing retrievals with and without a correction for the slit function. The applied correction varies from a few % to over 20% of the mean atmospheric signal, depending on the thickness of the ice layer. The resulting CH<sub>4</sub> and CO total columns are shown on a daily basis in Fig. 7, since the thickness of the ice layer varies strongly in time. In order to avoid influences of other time-dependent events, such as seasonal variation of CH<sub>4</sub> sources and sinks or polluted areas, only the retrieved total columns over the Sahara are taken into account, since the CH<sub>4</sub> and CO variation due to atmospheric processes is expected to be low in this region (Houweling et al., 1999). Figure 7a shows the results for CH<sub>4</sub>, where, for each day, the CH<sub>4</sub> total columns are normalized to the mean surface elevation of the corresponding SCIAMACHY pixel and then averaged over the Sahara. Note that this is a larger area than that used to determine the correction for the slit function (see Sect. 3). The difference between retrievals with and without slit-function correction is clearly visible. The CH<sub>4</sub> total columns retrieved with a correction for the slit function show an almost constant behaviour in time, in good agreement with calculations by the TM3 model. The trend in the CH<sub>4</sub> total columns for retrievals without slit-function correction resembles the loss in the measured total signal for this period, corresponding to the growth of the ice layer (see Fig. 2). The differences between retrievals with and without correction for the slit function range from ~6% shortly after a decontamination to 17.5% four months later, in December 2003. Although this figure only shows results for the Sahara, the retrieved total columns for Australia show the same effect: the differences in the CH<sub>4</sub> total columns increase from ~3% at 1 September to 18% in December 2003. The CH<sub>4</sub> total columns with the correction for the slit function show good agreement with TM3 model calculations (see also Fig. 3).

Figure 7b shows the results for the retrieved CO total columns. A strong correlation with the loss in the measured total signal due to the growing ice layer, as is present for CH<sub>4</sub>, cannot be seen for CO, but Fig. 7c shows the difference between the CO total columns retrieved without and with correction for the slit function respectively, relative to the CO total columns with slit-function correction. It can be seen that the relative difference correlates well with the loss in the total signal, indicating that the retrieved CO total columns are also clearly affected by the broadening of the slit function due to the growing ice layer. Differences between retrieved CO total columns with and without correction for the slit function range from ~10% shortly after a decontamination to ~35% four months later in December 2003. Using

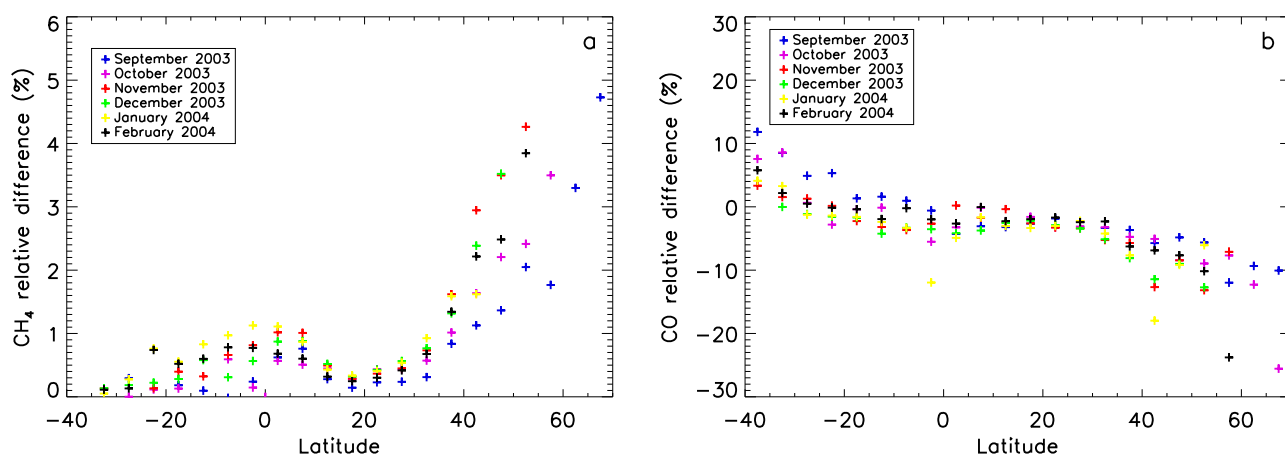


**Fig. 8.** The relative difference between the total columns retrieved without and with correction for the orbital variation of the dark signal respectively, for each month between September 2003 and February 2004. The data shown are the monthly mean total columns averaged per 5° latitude bin, between longitudes 30° W and 60° E. **(a)** The CH<sub>4</sub> total columns, normalized to the mean surface elevation of the corresponding SCIAMACHY pixel prior to averaging over a whole month of data. It is clearly seen that not correcting for the orbital variation of the dark signal leads to CH<sub>4</sub> columns that are up to ~4% higher on the Northern hemisphere compared to results including this correction. **(b)** The CO total columns, showing an effect opposite to that for CH<sub>4</sub>.

the CO total columns over Australia instead of the Sahara, results in similar values. While the differences for CH<sub>4</sub> are significantly larger than the current accuracy of the retrieved CH<sub>4</sub> total columns of a few %, the differences for CO are comparable to the current accuracy of the retrieved CO total columns (cf. Dils et al., 2005; Straume et al., 2005). However, the clear trend in Fig. 7c strongly suggests that the precision of the CO retrievals is much better than the current CO accuracy. Thus, although the correction for the slit function may seem less important for CO than for CH<sub>4</sub>, Fig. 7 shows that the total columns of both species are significantly affected by the ice layer.

## 5.2 Effects of the dark signal orbital variation

Although the orbital variation of the dark signal is much smaller than the slit-function correction, typically  $\lesssim 2\%$  of the measured atmospheric signal, it does have an effect on the retrieved columns, especially at Northern latitudes where the deviation of the actual dark signal from the measured dark signal reaches its largest values (Sect. 2). The effect of the variation of the dark signal over the orbit has been tested by performing retrievals with and without a correction for the orbital variation. This correction is taken from the data base set up by Kleipool (2004a). To demonstrate the effect of the orbital variation on the retrieved columns, monthly-averaged data have been investigated for the period September 2003–February 2004. Only the region between longitudes 30° W and 60° E has been investigated, since it has a good data coverage and large regions with high signal-to-noise ratio.

Since both the retrievals with and without correction for the orbital variation do include a correction for the slit func-

tion, which is much larger than the orbital variation itself, the two data sets should in principle not show a time-dependent behaviour due to the ice growth. This is true for the retrieved total columns including the correction for the orbital variation, which is done on an orbital basis. However, some time dependency is expected for the retrieved total columns without the correction for the orbital variation. Firstly, the orbital variation is linearly dependent on the measured signal, which decreases in time due to the ice growth. Secondly, the orbital variation is defined as a function of orbit phase, with orbit phase 0 corresponding to the start of the night side. Since phase 0 changes seasonally, this is expected to cause small time-dependent behaviour in the retrieved total columns without a correction for the orbital variation as a function of latitude. Therefore also the differences between the two data sets are expected to show some small time-dependent behaviour.

Figure 8a shows the relative differences between the monthly averaged CH<sub>4</sub> total columns without and with correction for the orbital variation respectively, in percentages of the retrievals with this correction. The results are shown as a function of latitude, where data within 5 degree latitude bins have been averaged prior to determining the differences. A clear increase in the relative difference can be seen towards Northern latitudes for all months, as expected. The difference is  $\gtrsim 2\%$  for latitudes  $\gtrsim 45^\circ$  N, and increases to ~4–5% at high Northern latitudes. This is a significant effect, since Fig. 4 showed typical differences between retrieved CH<sub>4</sub> and TM3 calculations of  $\lesssim 2\%$  outside the region between  $\sim 5^\circ$  S and  $\sim 15^\circ$  N (see Sect. 4.1). Similar values for the accuracy of the CH<sub>4</sub> total columns are reported by Gloudemans et al. (2004) and Dils et al. (2005).

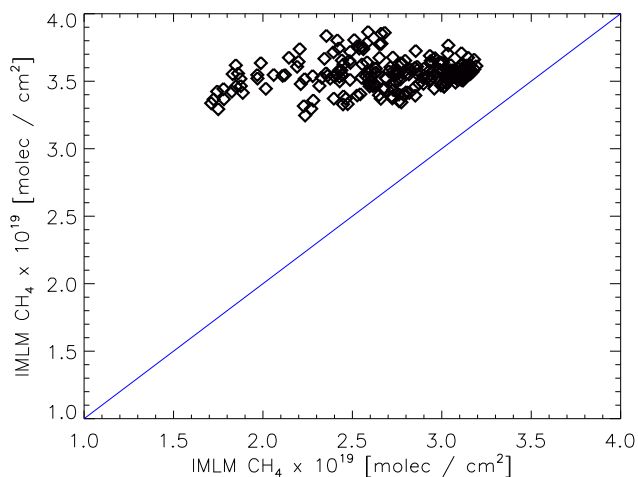


**Fig. 9.** The effect of 1 dead pixel on the CH<sub>4</sub> retrievals for orbit 10067 on 2 February 2004. The y-axis shows the CH<sub>4</sub> total columns when this dead pixel is not used in the retrievals. The x-axis shows the corresponding values when this pixel is included in the retrievals. The blue solid line denotes the expected 1:1 correlation. The deviation from the expected 1:1 correlation is different for each dead pixel (cf. Kleipool, 2004b).

The bump between  $\sim 15^\circ$  S and  $\sim 10^\circ$  N correlates well with the change in reflectance in this latitude range. Lower reflectances correspond to a lower signal level, resulting in a larger relative effect of the orbital variation, whereas higher signal levels result in a smaller effect. However, Fig. 8 shows that variations in the reflectance do not cause relative differences of more than  $\sim 1\%$ , which is much lower than the differences seen above  $\sim 45^\circ$  N. This strengthens the conclusion that the increase in the relative differences at high Northern latitudes are due to the increase in the dark signal over the orbit. Some differences between the different months are visible, but these are smaller than or comparable to the current accuracy of the CH<sub>4</sub> retrievals and are likely due to a combination of ice growth in time and the seasonal variation of the time of eclipse.

For CO, the effect of the orbital variation of the dark signal is not as evident as for CH<sub>4</sub>. In Fig. 8b, a decrease in the relative difference of the CO total columns without and with a correction for the orbital variation, can be seen towards higher latitudes for all months. However, the differences are generally within 15%, corresponding to the accuracy of the monthly-averaged retrieved CO total columns (Sect. 4.2 and Table 1). The apparent trend in the relative differences for CO is opposite to that for CH<sub>4</sub> (Fig. 8). This is probably due to the many CH<sub>4</sub> lines in channel 8, which are often (partially) overlapping with the much weaker and scarcer CO lines. This requires the CO lines to be fitted simultaneously with the CH<sub>4</sub> lines, indicating that the retrieved CO total columns may be influenced by the fit to the CH<sub>4</sub> lines in a non-linear way. Higher CH<sub>4</sub> total columns may fill in part

of the CO absorption lines, leading to lower retrieved CO total columns, but lower CH<sub>4</sub> total columns do not necessarily result in higher retrieved CO total columns as e.g. can be seen in Sect. 5.1. Although the effect of the orbital variation does not exceed the current accuracy of the retrieved CO total columns, the clear trend seen for all six months strongly suggests that the precision of the CO retrievals is much better, as is also indicated by the slit-function effect in Sect. 5.1 and Fig. 7. Thus, it is important to also correct the CO total columns for the orbital variation.

### 5.3 Effects of the dead pixels

The previous sections show that both the orbital variation and the growth of the ice layer result in a systematic, time-dependent effect on the retrieved columns. The dead detector pixels in SCIAMACHY's channel 8 are not expected to result in systematic effects. Although the number of dead pixels increases in time due to radiation damage (Kleipool et al., 2005<sup>2</sup>), the effect of dead pixels does not depend on their total number but on their spectral location. A pixel that does not sample (part of) an absorption line, is not expected to have an effect on the retrieved total columns, whereas a pixel that lies at the centre of an absorption line can affect the retrievals in two different ways: it can affect the retrieved total columns of the corresponding molecule and/or the retrieved total column of a different species, since the absorption lines of all molecules are fitted simultaneously.

In the case of CO, only a few absorption lines are present in the wavelength range of channel 8. These lines are most of the time barely above the noise level, many times weaker than the (often overlapping) CH<sub>4</sub> lines in the same spectra. Thus, even without dead pixels, retrieval of CO total columns from SCIAMACHY spectra is difficult. The presence of dead pixels and the corresponding loss of spectral information further complicates the CO retrievals. Unfortunately, a significant number of dead pixels are already located at or near the centre of CO lines. Therefore, there is a realistic possibility that an insufficient number of good detector pixels is left to retrieve accurate CO total columns well before the end of SCIAMACHY's life time.

On the other hand, the wealth of strong CH<sub>4</sub> lines in the wavelength range of SCIAMACHY's channel 8, ensures that the CH<sub>4</sub> retrievals are not easily influenced by dead pixels, as long as the dead pixels are not used when fitting the SCIAMACHY spectrum. However, Fig. 9 shows that the CH<sub>4</sub> retrievals are affected significantly, when this is not done correctly.

Thus, in order to perform accurate CO and CH<sub>4</sub> retrievals, a good identification of the dead pixels is required. There are two complications in deriving such a dead pixel mask. The first is the fact that detector pixels are damaged by radiation, mostly resulting in an abrupt change in their dark signal. Although detection of such dead pixels is relatively easy, it

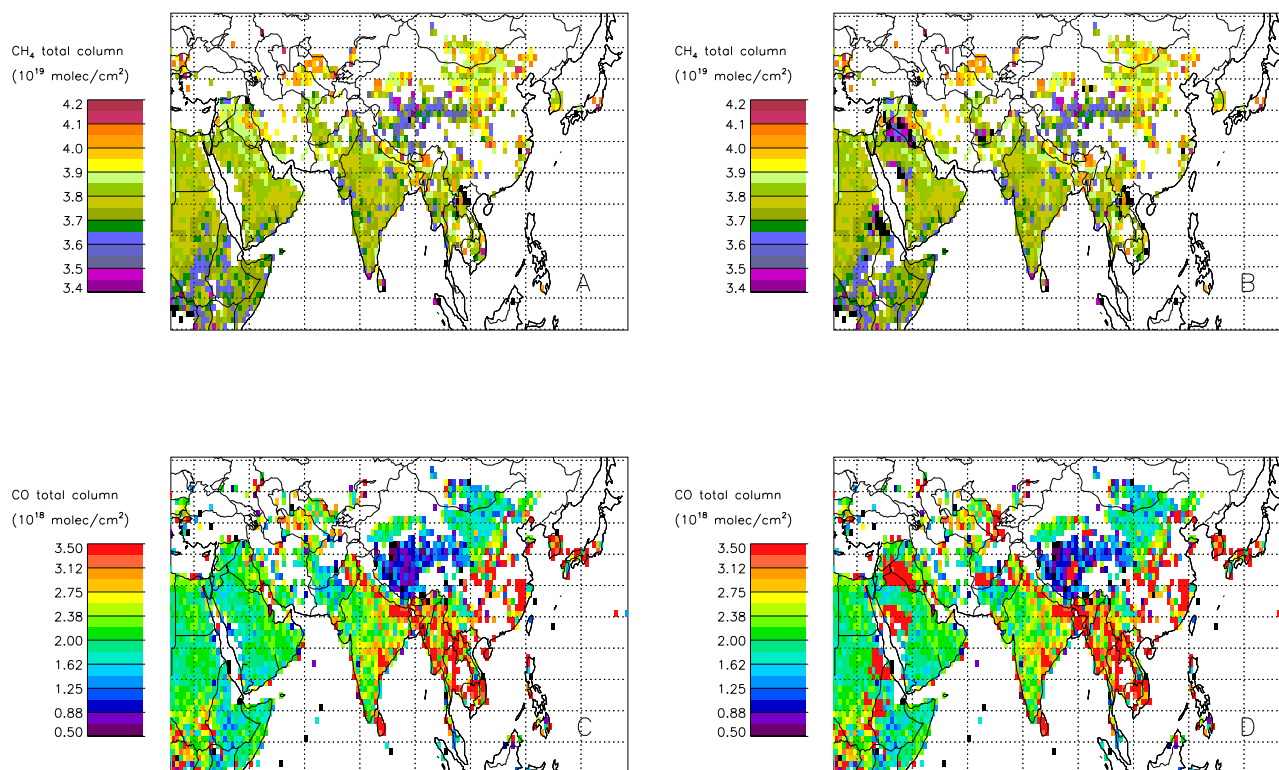


**Fig. 10.** Effect of not removing 1 dead pixel on the retrieved CH<sub>4</sub> and CO total columns over Asia and the Middle East for February 2004. (a) Monthly-averaged CH<sub>4</sub> total columns masking all dead pixels correctly. (b) Monthly-averaged CH<sub>4</sub> total columns omitting one dead pixel in the pixel mask for a period of 12 orbits ( $\sim 0.85$  day). (c) As panel a, but for CO. (d) As panel b, but for CO.

results in a slow but almost constant increase of dead pixels over time.

The second problem is that a significant number of bad detector pixels in channel 8 show regular jumps between two or more discrete levels of the dark current on timescales varying from less than  $\sim 1$  second to several days or longer. This implies that for some pixels the dark current during the SCIAMACHY measurement on the day side may be significantly different from the reference dark current measured at the night side. The size of these jumps can vary from values comparable to the noise in the dark current measurements to values comparable to the dark current itself. These so-called Random Telegraph Signal (hereafter: RTS) pixels can only be detected if the dead pixel identification algorithm includes a statistical constraint.

In order to deal with this, an algorithm has been developed that derives a dead pixel mask from the instrument calibration data for each orbit, which includes the physical characteristics of the detector pixels such as the dark signal. Then, a statistical method is used to filter out noise and to detect the so-called RTS pixels by including the information from the last 50 orbits, corresponding to  $\sim 3.5$  days. This will ensure that radiation-damaged pixels as well as RTS pixels are detected quickly and accurately.

The dead pixel mask used in the current retrievals only masks a pixel if its physical characteristics are bad for more than 25% of this period. This mask has been tested and works well: analyzing retrievals for a whole year, only a few dead pixels have been found that are not masked. For each of these pixels, this is only the case for a period of  $\sim 1$  day, after which each of them is masked correctly. Putting stronger constraints on the physical characteristics leads to a significantly larger number of dead pixels, including pixels that are still performing reasonably, further complicating the retrievals in channel 8. Therefore, it occasionally happens that a dead pixel does not appear in the pixel mask instantly, but only after  $\sim 1$  day. The current dead pixel mask is still being checked regularly and the current constraints may have to be adapted over time, to maintain a good performance.

However, even missing one pixel in the dead pixel mask for such a short period can have a significant effect on the retrievals. An example of this effect is shown for one such pixel, which is dead based on its physical quantities, but does not show up in the dead pixel mask until after  $\sim 0.85$  day or equivalently, 12 SCIAMACHY orbits. This pixel is located at the position of a CH<sub>4</sub> line, but not near a CO line. Figure 10 shows the results for retrievals with and without masking this dead pixel during its  $\sim 0.85$  day period in

**Table 1.** Summary of retrieval results in different spectral windows.

#	Window $\lambda$ (nm)	(IMLM-TM3)/TM3	(IMLM-MOPITT)/MOPITT	Ice growth effect		Effect of Orbital variation	
		CH <sub>4</sub> <sup>a</sup> (%)	CO <sup>a</sup> (%)	CH <sub>4</sub> <sup>b</sup> (%)	CO <sup>b</sup> (%)	CH <sub>4</sub> <sup>c</sup> (%)	CO <sup>c</sup> (%)
1	2321–2334	$\lesssim 2$	<15	6–17.5	10–35	<5	$\lesssim 15$
2	2327–2339	$\lesssim 2$	$\lesssim 15$	8–19.5	15–46	<5	$\lesssim 15$
3	2354–2370	$\lesssim 3$	$\lesssim 30$	6–18	2–25	<13	$\lesssim 30$

<sup>a</sup> For monthly-averaged total columns only. Differences for daily data are somewhat larger.

<sup>b</sup> Based on daily averaged total columns over the Sahara (Sect. 5.1).

<sup>c</sup> Based on monthly-averaged total columns between 30° W and 60° E (Sect. 5.2).

February 2004, and then averaging all retrieved CH<sub>4</sub> and CO total columns for that whole month. Comparing retrievals with and without masking this pixel clearly shows that it creates artificially low CH<sub>4</sub> columns in some areas, but it may not be that obvious that something is wrong from Fig. 10b only. Similarly, looking at Fig. 10d only, may lead to the conclusion that enhanced CO emission is seen over Iraq.

In this case, the retrievals of the individual orbits clearly indicate that something is wrong, by means of the large fit residuals. In fact, most of the time the few dead pixels that are missed are easily identified, since they cause large fit residuals and unrealistic values for the retrieved CH<sub>4</sub> and/or CO total columns. However, a few cases have been found where a pixel with truly bad physical characteristics still gives good fit residuals. In particular, RTS pixels with a low noise level could display such a behaviour. Investigation of the effect of one such dead pixel, leads to similar results as seen in Fig. 10: enhanced CO emission is seen over India, which disappears when this pixel is masked out. In the unlikely case that such a pixel is missed by the dead pixel mask, a good way to detect such dead pixels is by comparing retrievals from different wavelength ranges (see Sect. 5.4).

These results indicate that the identification of dead pixels is best done by monitoring their physical behaviour, but inspecting the retrievals afterwards for strange anomalies remains important. Identification of dead pixels by means of fit residuals only appears insufficient and may lead to misinterpretation of the results.

#### 5.4 Effect of retrieval windows

The results presented in the previous sections are based on retrievals in a single spectral window of SCIAMACHY's channel 8 between 2321–2334 nm (hereafter: window 1). Since this is not the only part of channel 8 that contains CO and/or CH<sub>4</sub> absorption lines, two other spectral windows, containing both CH<sub>4</sub> and CO lines, have been investigated. The results for all three windows are summarized in Table 1.

Window 2 covers the range 2327–2339 nm, and is chosen for the presence of strong CO lines that are relatively

unaffected by the dead pixels. It overlaps partially with window 1 which has been used so far and thus similar results are expected. Indeed, the retrieved CH<sub>4</sub> total columns are very similar to those from window 1, with monthly-averaged CH<sub>4</sub> results also differing from TM3 calculations by  $\lesssim 2\%$ . Comparisons of monthly-averaged CO results with MOPITT measurements show a good agreement between the two data sets, with differences within  $\sim 15\%$ .

The differences between retrievals with and without correction for the slit function vary between  $\sim 8\%$  and  $\sim 19.5\%$  for CH<sub>4</sub> and between  $\sim 15\%$  and  $\sim 46\%$  for CO. This may suggest a slightly thicker ice layer in this wavelength range compared to window 1.

The effect of the orbital variation of the dark signal is also similar to that in window 1, i.e. relative differences of up to  $\sim 4\text{--}5\%$  for CH<sub>4</sub> and up to  $\sim 15\%$  for CO at high Northern latitudes.

Window 3 ranges from 2354–2370 nm. This window is similar to the spectral range used by Buchwitz et al. (2004a) and contains CO lines from the *P*-branch, whereas the other windows contain *R*-branch CO lines. The monthly-averaged CH<sub>4</sub> total columns compare well with TM3 calculations and with results from the other two windows, although the differences with TM3 of  $\lesssim 3\%$  on the Southern Hemisphere are slightly larger than for window 1 and 2, and the deviation from TM3 seems to increase somewhat for high Northern latitudes. Comparisons of monthly-averaged CO results with MOPITT measurements result in deviations of  $\sim 30\%$ , larger than for the other two windows. Here, the retrieved CO total columns are mostly lower than those from MOPITT, whereas window 1 shows total columns somewhat larger and window 2 somewhat lower than MOPITT.

The effect of the broadening of the slit function due to the growing ice layer ranges from  $\sim 6\%$  to  $\sim 18\%$  for CH<sub>4</sub> in window 3, comparable to that of the other two windows. Although the atmospheric signal in this wavelength range is lower than in the other two windows, the slit-function broadening causes a relative effect on the CH<sub>4</sub> total column, thus explaining the similarity with the other two windows. For CO the difference between retrievals with and without

correction for the slit function shows no clear trend in time and ranges from  $\sim 2\%$  at the beginning of September 2003 to  $\sim 25\%$  around mid December, to  $\sim 20\%$  in early January just after the decontamination. This is probably related to the dead pixels in window 3, resulting in few CO lines that are unaffected. One particular pixel, which lies at the center of a strong CO line, causes the retrieval algorithm to give a wrong fit to the remaining detector pixels containing parts of the other CO lines. This probably explains the low retrieved CO total columns for window 3.

The effect of the orbital variation of the dark signal in window 3 is larger than in the other windows and can be up to  $\sim 13\%$  for CH<sub>4</sub> at high Northern latitudes. For CO, the effect is also larger than in the other windows, up to  $\sim 30\%$ , increasing towards Northern latitudes, whereas it is decreasing for the other windows. As for the other windows, the relative difference for CO is comparable to the accuracy of the CO total columns, making the effect of the orbital variation less pronounced for CO than for CH<sub>4</sub>. The larger effect of the orbital variation and the increasing differences for CO are probably due to the lower atmospheric signal in this wavelength range compared to the other windows (see Fig. 1). The lower signal introduces a larger effect on the retrieved total columns from window 3 for calibration issues with wavelength independent behaviour. The absolute values of the orbital variation of the dark signal show only a weak dependency on wavelength, thus explaining the larger relative differences in window 3. The lower atmospheric signal in window 3 also requires a better calibration, and thus the retrieved CH<sub>4</sub> and CO total columns may suffer from larger uncertainties. In addition, the dead pixels may play a role for CO in this window.

The number of dead pixels in all three windows are comparable, but it depends on the spectral location of these pixels whether the retrievals in one window give better results than in the other. The good agreement of the retrieved CH<sub>4</sub> total columns in all three windows gives some indication that in terms of dead pixels no window is preferred over another for the considered time period, and that no dead pixels that are important for the CH<sub>4</sub> retrievals are missed by the dead pixel mask. For CO, it seems that window 3 is preferred less than window 1 and 2, but using only part of window 3 results in CO total columns that are more in agreement with the results from the other two windows. This is due to a strong H<sub>2</sub>O line overlapping with one of the stronger CO lines in this window. All three windows contain strong H<sub>2</sub>O absorptions, but it depends on the position of the lines whether they will influence the retrieved CO and CH<sub>4</sub> total columns. In general there is a good correlation between the retrieved H<sub>2</sub>O total columns from different spectral windows, but there are cases with substantial differences too. This can also influence the retrieved total columns, especially for CO. Thus, using different windows in SCIAMACHY's channel 8 seems a good way to verify the retrieved CH<sub>4</sub> and CO total columns and thus improve their accuracy.

## 6 Discussion

The previous sections show that the growing ice layer, the orbital variation of the dark signal, and the dead pixels can cause significant errors in the retrieved CH<sub>4</sub> and CO total columns, when no or inaccurate corrections are taken into account. The nature of each of these effects is different. Whereas the effect of the growing ice layer varies strongly on the order of days, the effect of the orbital variation of the dark signal shows almost no time dependency. Also, both the growing ice layer and the orbital variation cause systematic effects in the retrieved CH<sub>4</sub> and CO total columns, whereas the effect of the dead pixels is rather unpredictable: some dead pixels show a random effect, some more systematic, and others no effect at all. Applying accurate corrections for these instrument calibration problems significantly improves the retrieved CH<sub>4</sub> and CO total columns.

Although the instrument calibration problems discussed in this paper have the largest impact on the retrieved total columns in SCIAMACHY's channel 8, additional smaller problems exist. As mentioned in Sect. 2, the dark signal decreases in time due to the growing ice layer and is currently measured for every SCIAMACHY orbit. However, the dark signal measurements are not available for every orbit for which SCIAMACHY data is present, due to incomplete data distribution and different versions of the distributed data. This may lead to small inaccuracies in the retrieved total columns, especially right after decontamination, when the dark signal is dropping fastest due to the ice growth. These are not expected to be larger than a few percent, which is within the current accuracy of the retrieved CH<sub>4</sub> and CO columns. Another possible error source is the non-linearity as reported by Kleipool (2003b). For channel 8 this effect is small and errors in the retrieved total columns of less than a few percent are expected. A more detailed calculation of these effects will be provided in a future paper. The instrument calibration issues mentioned in this paper apply to both SCIAMACHY's channels 7 and 8. Channel 7 also suffers from an additional serious problem, caused by a light leak.

In Sects. 5.3 and 5.4 it is mentioned that comparison of retrievals in different wavelength ranges gives additional information on the accuracy of the retrieved total columns. Here, only retrievals in SCIAMACHY's channel 8 have been discussed. For CH<sub>4</sub>, useful independent information can also be derived from SCIAMACHY's only other near-infrared channel 6, which covers the wavelength range 1000–1750 nm. This channel does not have an ice layer on its detector, and is not hampered by the orbital variation of the dark signal, due to the much higher atmospheric signal in this wavelength range. However, the spectral window containing CH<sub>4</sub> lines contains more dead pixels than in channel 8, non-linearity plays an important role, and scattering in the atmosphere complicates the retrieval. Nevertheless, CH<sub>4</sub> total column retrievals from channel 6 are foreseen for comparison with the CH<sub>4</sub> total columns presented in this paper.

## 7 Conclusions

In this paper, the effects of three important instrument calibration issues on the retrieved CH<sub>4</sub> and CO total columns from SCIAMACHY's channel 8 are discussed: the broadening of the slit function due to the growing ice layer on the detector, the variation of the dark signal over the orbit, and the dead detector pixels. The main conclusions are as follows:

- The CH<sub>4</sub> and CO total columns retrieved with the IMLM retrieval algorithm, including corrections for all known instrument calibration issues, compare well with calculations from the atmospheric chemistry transport model TM3 and independent measurements from the MOPITT instrument on board the EOS-TERRA satellite.
- The slit-function broadening due to the growing ice layer causes a time-dependent systematic effect on both the CH<sub>4</sub> and CO total columns. For CH<sub>4</sub>, this effect is much larger than the precision of ~1–2% required to detect CH<sub>4</sub> sources and sinks. The clear trend seen for CO, corresponds well with the loss in the total signal, indicating that also CO is significantly affected.
- The orbital variation of the dark signal also causes a systematic effect, but has only a small time dependency. This effect is much smaller than the effect of the slit function, but is still significant for both CH<sub>4</sub> and CO, especially at high Northern latitudes.
- The effect of the dead pixels on the retrieved total columns is unpredictable and depends on the spectral position of each individual dead pixel. Therefore, this effect is difficult to quantify in a general sense. An accurate algorithm which identifies the dead pixels for every orbit is required in order to avoid misinterpretation of the retrieved total columns. The dead pixel mask used in the IMLM retrieval is based on the physical characteristics of the detector pixels and works well. Nevertheless, inspecting the fit residual remains important since it provides additional information. However, a dead pixel mask based on fit residuals only is insufficient.
- Retrievals in different wavelength ranges within SCIAMACHY's channel 8 give similar results for CH<sub>4</sub>, but show some differences for CO. This is probably due to the scarcity and weakness of the CO lines in combination with the dead pixels, which complicates the CO retrievals significantly.
- Comparison of retrievals in different wavelength ranges provides a useful tool to detect imperfections in the applied instrument calibration corrections and helps to improve the quality of the retrieved total columns.

*Acknowledgements.* The authors would like to thank the SCIAMACHY and ENVISAT teams who have participated in the planning, building, launching, and operating of the SCIAMACHY instrument. They thank the Netherlands SCIAMACHY Data Center (NL-SCIA-DC) for providing us data and processing services. They also thank R. Hoogeveen, S. Houweling, and A. Maurellis at SRON for useful discussions. The MOPITT data presented in this paper were obtained from the NASA Langley Research Center Atmospheric Sciences Data Center. The work performed for this publication is (partly) financed by the Netherlands Agency for Aerospace Programmes (NIVR) and the European Commission (Fifth Framework Programme on Energy, Environment, and Sustainable Development, Contract no. EVG-1-CT-2002-00079, project EVERGREEN).

Edited by: H. Kelder

## References

- Barret, B., Turquety, S., Hurtmans, D., et al.: Global carbon monoxide vertical distributions from spaceborne high-resolution FTIR nadir measurements, *Atmos. Chem. Phys. Discuss.*, 5, 4599–4639, 2005,  
**SRef-ID: 1680-7375/acpd/2005-5-4599.**
- Beer, R., Glavich, T. A., and Rider, D. M.: Tropospheric emission spectrometer for the Earth Observing System's Aura satellite, *Applied Optics*, 40, 2356–2367, 2001.
- Buchwitz, M. and Burrows, J. P.: Retrieval of CH<sub>4</sub>, CO, and CO<sub>2</sub> total column amounts from SCIAMACHY near-infrared nadir spectra: Retrieval algorithm and first results, in *Remote Sensing of Clouds and the Atmosphere VIII*, edited by: Schäfer, K. P., Comeron, A., Carleer, M. R., and Picard R. H., *Proceedings of SPIE*, 5235, 375–388, 2004.
- Buchwitz, M., de Beek, R., Bramstedt, K., et al.: Global carbon monoxide as retrieved from SCIAMACHY by WFM-DOAS, *Atmos. Chem. Phys.*, 4, 1945–1960, 2004a,  
**SRef-ID: 1680-7324/acp/2004-4-1945.**
- Buchwitz, M., de Beek, R., Burrows J. P., et al.: Atmospheric methane and carbon dioxide from SCIAMACHY satellite data: initial comparison with chemistry and transport models, *Atmos. Chem. Phys.*, 5, 941–962, 2005,  
**SRef-ID: 1680-7324/acp/2005-5-941.**
- Buchwitz, M., de Beek, R., Noël, S., et al.: Carbon monoxide, methane and carbon dioxide columns retrieved from SCIAMACHY by WFM-DOAS: year 2003 initial data set, *Atmos. Chem. Phys. Discuss.*, 5, 1943–1971, 2005,  
**SRef-ID: 1680-7375/acpd/2005-5-1943.**
- Clerbaux, C., Hadji-Lazaro, J., Turquety, S., Mégie, G., Coheur, P.-F.: Trace gas measurements from infrared satellite for chemistry and climate applications, *Atmos. Chem. Phys.*, 3, 1495–1508, 2003,  
**SRef-ID: 1680-7324/acp/2003-3-1495.**
- Deeter, M. N., Emmons, L. K., Francis, G. L., et al.: Operational carbon monoxide retrieval algorithm and selected results for the MOPITT instrument, *J. Geophys. Res.*, 108, D14, 4399–4409, 2003.
- de Mazière, M., Barret, B., Blumenstock, T., et al.: Comparisons between SCIAMACHY scientific products and ground-based FTIR data for total columns of CO, CH<sub>4</sub>, and N<sub>2</sub>O, in

- Proc. Second Workshop on Atmospheric Chemistry Validation of ENVISAT (ACVE-2), ESA/ESRIN, Frascati, Italy, 3–7 May 2004, (ESA SP-562, August 2004), ESC02MDM, 2004.
- Dentener, F., van Weele, M., Krol, M., Houweling, S., and van Velthoven, P.: Trend and inter-annual variability of methane emissions derived from 1979–1993 global CTM simulations, *Atmos. Chem. Phys.*, 3, 73–88, 2003,  
**SRef-ID: 1680-7324/acp/2003-3-73.**
- Dils, B., de Mazière, M., Blumenstock, T., et al.: Comparisons between SCIAMACHY and ground-based FTIR data for total columns of CO, CH<sub>4</sub>, CO<sub>2</sub>, and N<sub>2</sub>O, *Atmos. Chem. Phys. Discuss.*, 5, 2677–2717, 2005,  
**SRef-ID: 1680-7375/acpd/2005-5-2677.**
- Drummond, J. R. and Mand, G. S.: The Measurements of Pollution in the Troposphere (MOPITT) Instrument: Overall Performance and Calibration Requirements, *Journal of Atmospheric and Oceanic Technology*, 13, 314, 1996.
- Ehret, G. and Kiemle, C.: Requirements Definition for Future DIAL Instruments, Final Report, ESA RFQ reference: IMT-CSO/FF/fe/03.887; RFQ/3-10880/03/NL/FF, DLR reference: 3 472 749, DLR, 2005.
- Frankenberg, C., Platt, U., and Wagner, T.: Retrieval of CO from SCIAMACHY onboard ENVISAT: detection of strongly polluted areas and seasonal patterns in global CO abundances, *Atmos. Chem. Phys.*, 5, 1639–1644, 2005a,  
**SRef-ID: 1680-7324/acp/2005-5-1639.**
- Frankenberg, C., Platt, U., and Wagner, T.: Iterative maximum a posteriori (IMAP)-DOAS for retrieval of strongly absorbing trace gases: Model studies for CH<sub>4</sub> and CO<sub>2</sub> retrieval from near infrared spectra of SCIAMACHY onboard ENVISAT, *Atmos. Chem. Phys.*, 5, 9–22, 2005b,  
**SRef-ID: 1680-7324/acp/2005-5-9.**
- Frankenberg, C., Meirink, J. F., van Weele, M., Platt, U., and Wagner, T.: Assessing Methane Emissions from Global Space-Borne Observations, *Science (Science Express 17 March 2005)*, 2005c.
- Gloudemans, A. M. S., Schrijver, H., Straume, A. G., et al.: CH<sub>4</sub> and CO total columns from SCIAMACHY: Comparisons with TM3 and MOPITT, in Proc. Second Workshop on Atmospheric Chemistry Validation of ENVISAT (ACVE-2), ESA/ESRIN, Frascati, Italy, 3–7 May 2004 (ESA SP-562, August 2004), ESC02AG, 2004.
- Houweling, S., Kaminski, T., Dentener, F., Lelieveld, J., and Heimann, M.: Inverse modeling of methane sources and sinks using the adjoint of a global transport model, *J. Geophys. Res.*, 104, D21, 26 137–26 160, 1999.
- Houweling, S., Dentener, F. J., Lelieveld, J., Walter, B., and Dlugokencky, E. J.: The modeling of tropospheric methane: How well can point measurements be reproduced by a global model?, *J. Geophys. Res.*, 105, d7, 8981–9002, 2000.
- Kleipool, Q.: SCIAMACHY SODAP: Algorithm Specification for Dark Signal Determination, Tech. Report SRON-SCIA-PhE-RP-009, SRON, 2003a.
- Kleipool, Q.: SCIAMACHY: Recalculation of OPTEC5 Non-Linearity, Tech. Report SRON-SCIA-PhE-RP-013, SRON, 2003b.
- Kleipool, Q.: SCIAMACHY: Orbital Variation of dark signal, Tech. Report SRON-SCIA-PhE-RP-18, SRON, 2004a.
- Kleipool, Q.: SCIAMACHY: Evolution of Dead and Bad Pixel Mask, Tech. Report SRON-SCIA-PhE-RP-21, SRON, 2004b.
- Krijger, J. M., Aben, I., and Schrijver, H.: Distinction between clouds and ice/snow covered surfaces in the identification of cloud-free observations using SCIAMACHY PMDs, *Atmos. Chem. Phys. Discuss.*, 5, 815–845, 2005,  
**SRef-ID: 1680-7375/acpd/2005-5-815.**
- Lichtenberg, G. F., Kleipool, Q., Krijger, J. M., et al.: SCIAMACHY Level1 data: Calibration concept and in-flight calibration, *Atmos. Chem. Phys. Discuss.*, 5, in press, 2005.
- Rodgers, C. D.: *Inverse Methods for Atmospheric Sounding*, World Scientific, London, 2000.
- Schrijver, H.: Retrieval of carbon monoxide, methane and nitrous oxide from SCIAMACHY measurements, in Proc. ESAMS, European Symposium on Atmospheric Measurements from Space, ESA WPP-161 1, ESTEC, Noordwijk, The Netherlands, 285–294, 1999.
- Straume, A. G., Schrijver, H., Gloudemans, A. M. S., et al.: The global variation of CH<sub>4</sub> and CO as seen by SCIAMACHY, *Adv. Space Res.*, in press, 2005.